Original Paper

Near-Global Scale Retrieval of the Optical and Microphysical Properties of Clouds from Midori-II GLI and AMSR Data

Takashi Y. NAKAJIMA*[1,2], Hirohiko MASUNAGA*[3] and Teruyuki NAKAJIMA*[4]

Abstract

Various optical and microphysical properties of warm water-phase clouds as retrieved from the GLI and AMSR global datasets are presented. The results indicate that the retrieved effective particle radius at the cloud top was small (6 to $10\,\mu$m) not only over continental and coastal ocean areas, but also over the North Pacific Ocean. The ADEOS-II GLI-AMSR coupled analysis first yielded the vertical structure of the effective particle radius over middle-to-high latitude areas, which was not covered by TRMM TMI-VIRS. The results also show that the effective particle radius at the cloud top is comparable to or larger than that in the middle to bottom layers in areas where the effective radius at the cloud top is small. These features are very similar to those at the Namibian, East Asian, Californian, and Peruvian regions, which are known as non-precipitation areas. In addition, comparisons between cloud properties retrieved from GLI and MODIS revealed that the GLI-derived effective particle radius was smaller than that derived from MODIS. The GLI-derived effective radius had a single mode in the histogram at $12\,\mu$m, while the MODIS had a bi-modal structure at $10\,\mu$m and $14\,\mu$m as well as an inflection point at $18\,\mu$m. One of the reasons for this difference in the retrieved effective radii is considered to be the difference in wavelength used for retrieving the cloud effective particle radius, where GLI and MODIS used $3.7\,\mu$m and $2.1\,\mu$m, respectively.

Keywords : ADEOS-II, Global Imager (GLI), AMSR, Cloud Properties, Climate Change

1. Introduction

1.1 Significance of cloud studies

Clouds are one of the important observation targets for understanding climate change mechanisms. The International Panel on Climate Change (IPCC) Forth Assessment Report (AR4)[1] pointed out that clouds are still characterized by large uncertainties in the estimation of the energy balance on Earth. From this point of view, it is important to reveal the process of the growth of cloud droplets and their interaction with aerosols, as well as the global distribution of clouds and their microphysical properties. The importance of any factor directly and/or indirectly affecting the energy balance is expressed in terms of "radiative forcing", which is used for understanding how a range of human and natural factors contribute to the warming or cooling of the global climate. Radiative forcing is defined as the difference in energy balance between the pre-industrial and present epochs. Positive and negative values of radiative forcing indicate warming and cooling, respectively. For example, AR4 has reported that carbon dioxide, which is a greenhouse gas, has a radiative forcing value of $+1.66\,\mathrm{W/m^2}$ (warming), whereas the change of the cloud albedo associated with the change of the aerosol concentration in the atmosphere is $-0.7\,\mathrm{W/m^2}$ (cooling). This suggests that the warming effects of carbon dioxide are canceled in part by the cooling effects of clouds through changes in the aerosol concentration. However, the estimated radiative forcing due to the cloud albedo effect is still associated with large uncertainties regarding its value, which fluctuates in the range of -1.8 to $-0.3\,\mathrm{W/m^2}$. This uncertainty is mainly due to insufficient knowledge regarding cloud-aerosol interactions. Therefore, global-scale observations of clouds and aerosols, as well as the modeling of cloud-aerosol interactions, are important research activities in climate studies.

1.2 Advantages of the Midori-II cloud observations

The Global Imager (GLI) aboard the Midori-II satellite, which is known as the Advanced Earth Observing Satellite-II (ADEOS-II), is one of the Earth observation sensors suitable for achieving the objective mentioned above. This is because it has 36 channels in the range from the ultraviolet to the

thermal infrared region which enables us to retrieve the properties of clouds and aerosols, and a wide swath ($\sim$1600 km), which allows for frequent observations to be performed. The Instantaneous Field Of View (IFOV) is 1 km at the nadir looking for most channels and 250 m for the five channels corresponding to the LANDSAT Thematic Mapper (TM). The position and the bandwidth of each GLI channel were optimized by using radiative transfer simulations so as to retrieve the physical parameters with high accuracy[2]. The advantage of GLI with respect to cloud observations are summarized as follows.

(1) It was scientifically optimized on the basis of radiative transfer simulations[2].

(2) It has many channels in the range from the visible to the infrared region enabling cloud screening to be performed with high accuracy[3].

(3) It has three short-wave infrared (SWIR) channels (1.6, 2.2, and 3.7 μm), which allow for the precise surveillance of cloud properties[4].

(4) It has an oxygen-A band channel which is used for retrieving the geometrical thickness of clouds[5].

(5) The Advanced Microwave Scanning Radiometer (AMSR) is mounted aboard the satellite together with GLI. The coupled use of GLI and AMSR for remote sensing of clouds provides the vertical structure of the cloud droplet size (shown in this paper). The Tropical Rainfall Measuring Mission (TRMM) also includes the Visible and Infrared Scanner (VIRS) and the TRMM Microwave Imager (TMI). However, the GLI-AMSR observations have an advantage since they yield observations of middle-to-high latitude areas, which are not covered by VIRS-TMI.

In this paper, we discuss (3) and focus on the advantages of (5).

1.3 History of cloud observations based on satellite-borne imaging spectroradiometers

A number of studies have observed the optical and microphysical properties of clouds using satellite-borne imaging spectroradiometers. For example, Han et al. (1994)[6] retrieved the cloud optical thickness (τ_c) and the effective particle radius (r_e) near-globally using radiance data from the nadir looking of the Advanced Very High Resolution Radiometer (AVHRR) operated by the National Oceanic and Atmospheric Administration (NOAA). One of the interesting features reported by Han et al. (1994) is the contrast between the effective particle radius over continental areas and that over coastal ocean areas. In fact, the average effective particle radius is smaller over continental areas ($=8.5 \mu$m) than over coastal ocean areas ($=11.8 \mu$m). Nakajima and Nakajima (1995)[7] (hereafter, N&N) developed an algorithm which re-

trieved the cloud properties applicable to the whole AVHRR 2000-km swath and analyzed the "Ship-Tracks" phenomena which appeared off the coast of California. N&N found that the aerosol seeding from the ship resulted in a 17% decrease of the effective cloud particle radius (from 12 μm to 10 μm). Kawamoto et al. (2001)[8] extended the N&N algorithm so that the atmospheric water vapor effects included in the radiances measured with AVHRR are explicitly corrected using the effective water vapor profile calculated from objective analysis data, such as that from the European Centre for Medium-Range Weather Forecasts (ECMWF), the National Center for Environmental Prediction (NCEP), and the Japan Meteorological Agency Grid Point Value (JMA-GPV). Validations of the retrieved cloud properties have been performed by comparing satellite and aircraft data *in situ,* as well as satellite data with ground-based observations[7~9] The estimated retrieval errors were less than 10% for both τ_c and r_e. These previous studies demonstrated not only the possibility of performing cloud microphysics observations by satellite remote sensing, but also the usefulness of the results to climate change studies through the analysis of snapshot images (e.g., quantification of the ship track effect by N & N) and/or the analysis of time series of cloud properties in remotely sensed results and subsequent comparisons of global cloud distributions as determined from satellite remote sensing and General Circulation Model (GCM) outputs[10]. The Moderate Resolution Imaging Spectroradiometer (MODIS) aboard Terra (1999−) and Aqua (2000−), is a sensor similar to GLI. The MODIS atmosphere science team developed the cloud retrieval algorithm[11].

A synergetic use of the multispectral visible-to-infrared imager and the microwave scanner is one of the new aspects of cloud observation attempts in recent years. For example, Masunaga et al. (2002a, 2002b)[12][13] obtained the vertical structure of the effective cloud particle radius in warm water-phase clouds over low and middle latitude areas (35 degs north to 35 degs south) by using the visible-to-infrared imager and the microwave scanner aboard the Tropical Rainfall Measuring Mission (TRMM) satellite. Matsui et al. (2004)[14] examined the TRMM data in detail and revealed that the formation of warm rain is suppressed under highly stable atmospheric conditions regardless of the concentration of aerosols, whereas high aerosol concentrations suppress the formation of warm rain in low stability conditions.

1.4 Contents of this paper

This paper presents results of the microphysical properties of warm water-phase clouds as obtained from the GLI and AMSR cloud measurement missions. The theoretical background of the retrieval of the properties and the expected retrieved geophysical parameters are summarized in Section

2. The data used in the analyses are briefly summarized in Section 3. The typical results for the GLI cloud products and a comparison between the results obtained from GLI and MODIS are shown in Section 4 together with a discussion of the wavelengths used in the effective particle radius retrievals. The synergistic analysis of clouds performed using data from GLI and AMSR measurements, as mentioned in Sections 2 and 4, is one of the unique results which was not expected at the beginning of the GLI science mission. This paper presents for the first time the results of the coupled use of GLI and AMSR for cloud analysis.

2. Algorithm development

2.1 ATSK3r algorithm development

The algorithm used for retrieving the microphysical and optical properties of clouds from GLI-measured multispectral daytime data is named "ATSK3r (Atmospheric TaSK number 3, reflection method)" in the GLI mission flow chart. ATSK3r retrieves the cloud optical thickness, the effective particle radius, and the cloud top temperature (and/or cloud top height), from daytime visible, short-wave infrared, and thermal infrared channels. The ATSK3r algorithm was originally a part of the Comprehensive Analysis Program for Cloud Optical Measurement (CAPCOM) as developed from the N & N (1995) algorithm. CAPCOM is distributed under the Open Clustered Libraries for Atmospheric Science and Transfer of Radiation (OpenCLASTR) project (http://www.ccsr.u-tokyo.ac.jp/~clastr/index.html), operated by the Japanese atmospheric radiation community.

(1) Theoretical background of ATSK3r

The solar reflectance method utilizes non-absorbing visible (Vis) and water-absorbing short-wave infrared (SWIR) wavelengths, such as 1.6, 2.2 and 3.7 μm, for the simultaneous retrieval of the cloud optical thickness at the 0.5 μm wavelength and the effective particle radius. In this paper, we mainly discuss the solar reflectance method making use of GLI channels 13 (0.64 μm), 30 (3.715 μm), and 35 (10.8 μm). The effective particle radius of the clouds (r_e) is defined by

$$r_e \equiv \frac{\int_0^\infty r^3 n(r) dr}{\int_0^\infty r^2 n(r) dr}, \tag{1}$$

where $n(r)$ is the number size distribution as a function of the particle radius r. We used a log-normal size distribution in the calculations,

$$n(r) = \frac{c}{r} \exp\left[-\frac{(\ln r - \ln r_0)^2}{2\sigma_2}\right], \tag{2}$$

where c is a constant, r_0 is the mode radius, which is related to the effective particle radius as $r_e = r_0 e^{2.5\sigma_2}$, and σ is the log-standard deviation of the size distribution. Here, $\sigma = 0.35$ was assumed for marine stratocumulus clouds in our analyses. For the satellite signal simulation, we used an accurate and efficient radiative transfer scheme[15)16)] extended to include the thermal radiative transfer[17)]. We assumed a Lambert surface for the underlying surface. This assumption will not introduce a significant error in the analyses if we use an equivalent flux albedo for cloudy atmospheres[18)].

We retrieved τ_c at the 0.5-μm wavelength and r_e from GLI channels 13 and 30 on the basis of the fact that channels 13 and 30 primarily depend on the cloud optical thickness and the effective particle radius, respectively. Although the concept of the retrieval is simple, some difficulties occur when determining the cloud properties from the measured GLI spectral radiance. It is necessary to remove the unexpected radiation components (e.g. solar radiation reflected by the ground surface and thermal radiation emitted from the cloud layer and the ground surface) from the observed radiance. The ground reflectance largely contributes to the satellite signal in the full range of τ_c in channel 13, whereas it becomes important only if τ_c is less than 10 in channel 30. The radiance in channel 30 is influenced by the ground thermal radiation in the range of $\tau_c < 10$. These undesirable radiation components must be removed from the measured radiances by using the formulations provided in the next subsection.

(2) Formulations of the radiative components

According to the radiative transfer theory for parallel plane layers with an underlying Lambert surface, we remove the unexpected radiation components, such as the solar radiation reflected by the ground surface and the thermal radiation emitted from the cloud layer and the ground surface, from the satellite-received radiance, L_{obs}, in order to decouple the radiation component reflected by the cloud layer, L, as follows : for visible wavelength (0.678 μm, GLI channel 13),

$$L(Z_c, D_c, \tau_c, r_e ; \mu, \mu_0, \phi)$$
$$= L_{obs}(Z_c, D_c, \tau_c, r_e ; \mu, \mu_0, \phi)$$
$$- t(Z_c, D_c, \tau_c, r_e ; \mu)\frac{A_g}{1-r(Z_c, D_c, \tau_c, r_e)A_g}$$
$$t(Z_c, D_c, \tau_c, r_e ; \mu_0,)\frac{\mu_0 F_0}{\pi} \tag{3}$$

and for SWIR wavelength (3.715 μm, GLI channel 30),

$$L(w_u, w_c, \tau_c, r_e ; \mu, \mu_0, \phi)$$
$$= L_{obs}(w_u, w_c, \tau_c, r_e ; \mu, \mu_0, \phi)$$
$$- t(w_u, \tau_u, \mu)[1 - t(w_c, \tau_c, r_e ; \mu) - r(w_c, \tau_c, r_e ; \mu)]B(T_c)$$
$$- t(w_u, w_c, \tau_c, r_e ; \mu)\frac{1-A_g}{1-\bar{r}(w_u, w_c, \tau_c, r_e)A_g}B(T_g)$$
$$- t(w_u, w_c, \tau_c, r_e ; \mu)\frac{A_g}{1-\bar{r}(w_u, w_c, \tau_c, r_e)A_g}$$
$$t(w_u, w_c, \tau_c, r_e ; \mu_0)\frac{\mu_0 F_0}{\pi}$$

$$-L_{tml}(w_u, T_c)$$
$$-t(w_u, \tau_u, \mu)t(w_c, \tau_c, r_e, \mu)L_{tml}(w_d, T_g) \qquad (4)$$

where F_0 is the extraterrestrial solar flux, B is the Planck function, and τ, τ_c and τ_u are the optical thicknesses of the atmosphere, the cloud layer, and the atmosphere above the cloud layer, respectively. Furthermore, μ_0 and μ are the cosines of the solar and satellite zenith angles, respectively, ϕ is the azimuthal angle of the satellite relative to the sun, T_c is the cloud top temperature, and w_u, w_c, and w_d are the equivalent water vapor amounts of above cloud (u), cloud layer (c), and below cloud (d), which are defined as

$$w_{u,c,d} = \int_{z_1}^{z_2} w(z)(P(z)/P_g)^{0.5}(T_g/T(z)))^{0.9}dz \qquad (5)$$

where, z_1 and z_2 represent cloud top and top of atmosphere, cloud bottom and cloud top, ground level and cloud bottom, for the case of w_u, w_c, and w_d, respectively[8], $P(z)$ and $T(z)$ are the vertical profile of the air pressure and the air temperature as a function of the altitude z, P_g and T_g are the surface pressure and the temperature. Z_c and D_c are the top height and the geometrical thickness of the cloud, respectively. The transmissivity t, the plane albedo r, and the spherical albedo $\bar{r}$ are given by

$$t(\tau_c, r_e, \mu_0)$$
$$= \frac{1}{\pi}\int_0^{2\pi}\int_0^1 T(\tau_c, r_e ; \mu, \mu_0, \phi)\mu d\mu d\phi + e^{-\tau/\mu_0} \qquad (6)$$

$$r(\tau_c, r_e, \mu)$$
$$= \frac{1}{\pi}\int_0^{2\pi}\int_0^1 R(\tau_c, r_e ; \mu', \mu, \phi)\mu' d\mu' d\phi \qquad (7)$$

$$\bar{r}(\tau_c, r_e) = 2\int_0^1 r(\tau_c, r_e ; \mu)\mu d\mu, \qquad (8)$$

where $T(\tau_c, r_e ; \mu, \mu_0, \phi)$ and $R(\tau_c, r_e ; \mu', \mu, \phi)$ are bidirectional transmission and reflection functions respectively. The second term in Eq. (3) and the fourth term in Eq. (4) are ground-reflected radiation components, and the second and third terms in Eq. (4) are cloud and ground thermal radiation components. The fifth and sixth terms in Eq. (4) are active thermal correction components from the layers above and below the cloud, respectively. Multiple reflections between the ground surface and the upper layer are taken into consideration in Eqs. (3) and (4). However, this effect is sufficiently small to regard $\bar{r}(\tau_c, r_e) A_g$ as almost zero, especially for optically thin clouds and ground surfaces with low reflectance. On the contrary, with optically thick clouds and large ground albedo, this effect is relatively large at visible wavelengths since the large cloud spherical albedo reflects radiation from the ground surface, while the relatively large transmissivity allows this radiation component to be transmitted into space. These formulations are exact when we consider

monochromatic radiance. We further introduce a process of averaging of the variables in the formulations with respect to the wavelength. For example, t is averaged with a subchannel response function of GLI as

$$t = \sum_{n=1}^{N}\varphi n\left\{\sum_{k=1}^{M}(\xi_{n,k} \times t_{n,k})\right\}/\sum_{v=1}^{n}\varphi_n, \qquad (10)$$

where φ_n is the response function of the n-th subchannel wavelength for each GLI channel (we used φ_n values obtained from http://suzaku.eorc.jaxa.jp/GLI/index.html), $\xi_{n,k}$ is the weight of the k-th k-distribution, and $t_{n,k}$ is the transmissivity for the k-th k-distribution at the n-th wavelength. This averaging process, which was applied to Eqs. (3) and (4), introduces a non-negligible error into the case of thin cloud layers in which the spectral variation of $t_{n,k}$ becomes large. However, in most cases in which this process is applied, the error remains small, and it is possible to estimate the undesirable radiation components in Eqs. (3) and (4) by using spectrally averaged variables for each channel.

2.2 Combined GLI-AMSR algorithm

The effective radius retrieved from the GLI 3.715-μm channel is the cloud droplet size at nearly the cloud top due to the large imaginary index of refraction of water droplets at this channel. Contrastingly, the microwave scanner channels, on the other hand, contain information of cloud droplet size regarding the entire cloud layer. Thus, the coupled use of the visible-to-infrared and microwave radiometers for observing warm water-phase clouds can provide significant information pertaining to the vertical profiles of cloud properties. For example, it is possible to calculate the ratio of two kinds of effective particle radii, namely r_e_SWIR&Vis, which is obtained individually with the visible-to-infrared imager, and r_c_Mic&Vis, which is obtained through the coupled use of the microwave scanner and the visible-to-infrared imager, by using the following formulation

$$r_e\_\text{Mic\&Vis} \cong \frac{3}{2} \cdot \frac{W\_\text{Mic\&Vis}}{\tau_c}, \qquad (11)$$

where W_Mic&Vis and τ_c are the cloud liquid water path as obtained from AMSR retrieval and the cloud optical thickness obtained with GLI retrieval, respectively.

Midori-II was equipped with GLI and AMSR sensors. The former is a visible-to-infrared imager, while the latter a microwave scanner. Figure 1 presents the flow of the coupled algorithm of the GLI and AMSR analysis. First, the GLI and AMSR data are initialized in advance through a path-segment process in order to ensure the temporal and spatial registration matching of the two sensors. Next, the 0.678-, 3.715-, and 10.8-μm channels of the GLI retrieve the cloud optical thickness τ_c, the effective particle radius r_e_SWIR&Vis, and the cloud top temperature T_c in accordance to the algorithm
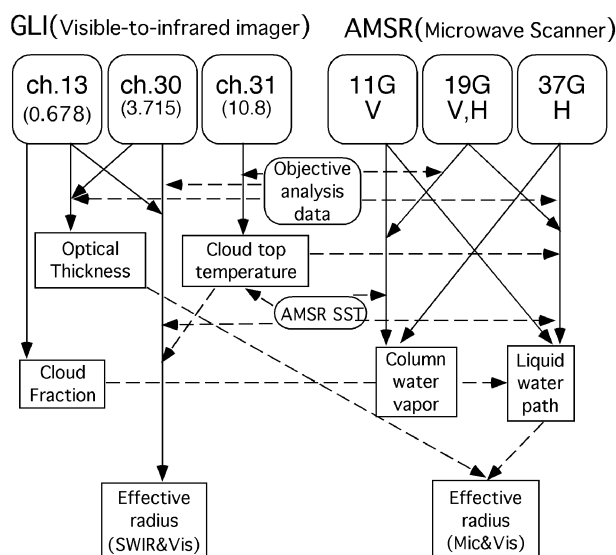
Fig. 1   Diagram of the coupled use of GLI and AMSR multi-spectral data used for retrieving the effective radii SWIR&Vis and Mic&Vis.

Table 1   Cloud parameters as retrieved from GLI, AMSR, and GLI＋AMSR.

	GLI	AMSR	GLI+AMSR
Cloud fraction	C.F.	-	-
Sea surface temperature		SST	
Cloud optical thickness	τ_c		
Effective particle radius	r_e_SWIR&Vis		r_e_Mic&Vis
Liquid water path		W_Mic&Vis	
Cloud top temperature	T_c		
Column water vapor		CWV	

mentioned in Section 2.1. Subsequently, the 11-, 19-, and 37-GHz channels of AMSR are used for calculating the column water vapor (CWV) and the liquid water path W_Mic&Vis by using the algorithm developed by Masunaga et al. (2002a)[12], with the help of T_c as derived from GLI and the cloud fraction (C.F.) at every AMSR IFOV in order to obtain a precise brightness temperature correction of the AMSR signals. Both the GLI and the AMSR analysis use the SST data obtained from the 5-day running mean of the AMSR-E aboard the Aqua satellite daily SST dataset. Thus, Eq. (11) outputs a different effective particle radius (τ_e_Mic&Vis) based on τ_c and W_Mic&Vis. Generally speaking, r_e_SWIR&Vis is the cloud droplet size at the cloud top and r_e_SWIR&Vis is the averaged droplet size for the entire cloud layer. Therefore, the ratio of r_e_Mic&Vis to r_e_SWIR&Vis is assumed to be an indicator of the vertical structure of the cloud droplet size. We define the effective particle radius ratio (ERR) as

$$ERR = r_e\_Mic\&Vis/r_e\_SWIR\&Vis. \qquad (12)$$

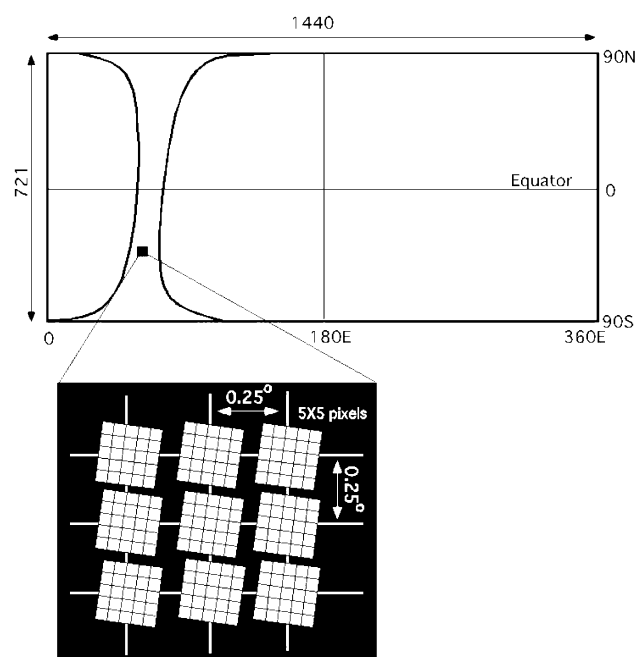Table 1 summarizes the parameters obtained from the GLI,

Fig. 2   Schematic view of the GLI Atmospheric Segment (ATSEG) dataset. The upper panel represents the global map, which has 1440×721 boxes with equal latitude and longitude. The interval of boxes is 0.25 degrees for both the latitude and the longitude, and each box is composed of 5×5＝25 pixels (lower panel).

AMSR, and GLI＋AMSR retrievals.

3.   Satellite data and ancillary data

We used a reduced-volume GLI radiance dataset named "Atmospheric segment (ATSEG) data", which comprises gridded data with equal longitude and latitude divisions. Each segment comprises a grid box with dimensions of 0.25× 0.25 degrees, so that the global dataset contains 1440×721 boxes. 5×5＝25 pixels of the GLI image are included in each segment element. Figure 2 illustrates the schematic view of the ATSEG data. Level-1b AMSR were used for the AMSR analysis. Two kinds of ancillary data were used in the retrievals for the purpose of supporting the GLI cloud retrieval algorithm. One of them is JMA objective analysis data. The vertical profiles of the pressure, the humidity, and the temperature for each GLI pixel were used. The other ancillary data is the 5-day running mean daily SST dataset derived from AMSR-E and provided by Keiji Imaoka from JAXA EORC. The SST data are needed for both the GLI and the AMSR analysis.

4. Results

4.1 GLI cloud properties for April 2003

Figure 3 (A) (B) (C) illustrates the warm water cloud parameters obtained with GLI in April 2003. The data are monthly averaged at every 0.25×0.25 degrees in latitude and longitude direction in the grid area. Figure 3 (A) shows that the cloud optical thickness τ_c is large at the east coast of North America, the middle part of South America, the northern parts of Europe, and the northern and southeastern parts of Asia. In these areas, the averaged τ_c was between 20 and 30. Furthermore, the values of τ_c are relatively large over the areas off the east coast of Asia (North Pacific Ocean) and between North America and Europe (North Atlantic Ocean). Figure 3 (B) shows that the effective particle radius r_c is smaller over continental and coastal ocean areas than over open ocean zones. These results are consistent with those obtained by Han et al. (1994)[6] and Kawamoto et al. (2001)[8]. It is found that the zones with small effective particle radius are spread over a wide area extending from East Asia to the North Pacific Ocean. This area corresponds to an area of dense aerosols arriving from East Asia. Here, this might be indicative of the indirect effects of aerosols on the cloud properties. This speculation is discussed again by using new results obtained from the coupled analysis of GLI and AMSR in Section 5. The cloud top temperature T_c Figure 3 (C) shows that T_c is high in low to middle latitude areas and low in high latitude areas.

4.2 Comparison between the results obtained from MODIS and GLI

MODIS aboard the Terra satellite was operated simultaneously with GLI throughout 2003. Thus, we compared the results regarding the cloud properties as obtained from GLI and MODIS. Figure 4 illustrates the correlation of the cloud parameters (τ_c and r_e) obtained from GLI and MODIS as standard products in April 2003. The difference of the observation time between GLI and MODIS is less than 100 minutes. In Figure 4, we can see a good correlation in the comparison of τ_c (correlation coefficient $R = 0.8$) and r_e ($R = 0.77$), although the values of r_e are larger in MODIS than in GLI, with a slope of 1.12. In order to analyze this difference, we prepared a histogram of the cloud properties. Figure 5 shows a comparison of the histograms of GLI and MODIS for both land and water areas (upper panels), land areas only (middle), and water areas only (lower). In Figure 5 (a), the mode values of τ_c in GLI and MODIS are very close to the values of τ_c up to 4, and the shapes of the histograms are similar. However, the histograms in Figure 5 (c) and (e) show that the mode value of τ_c from GLI (~ 4) is smaller than
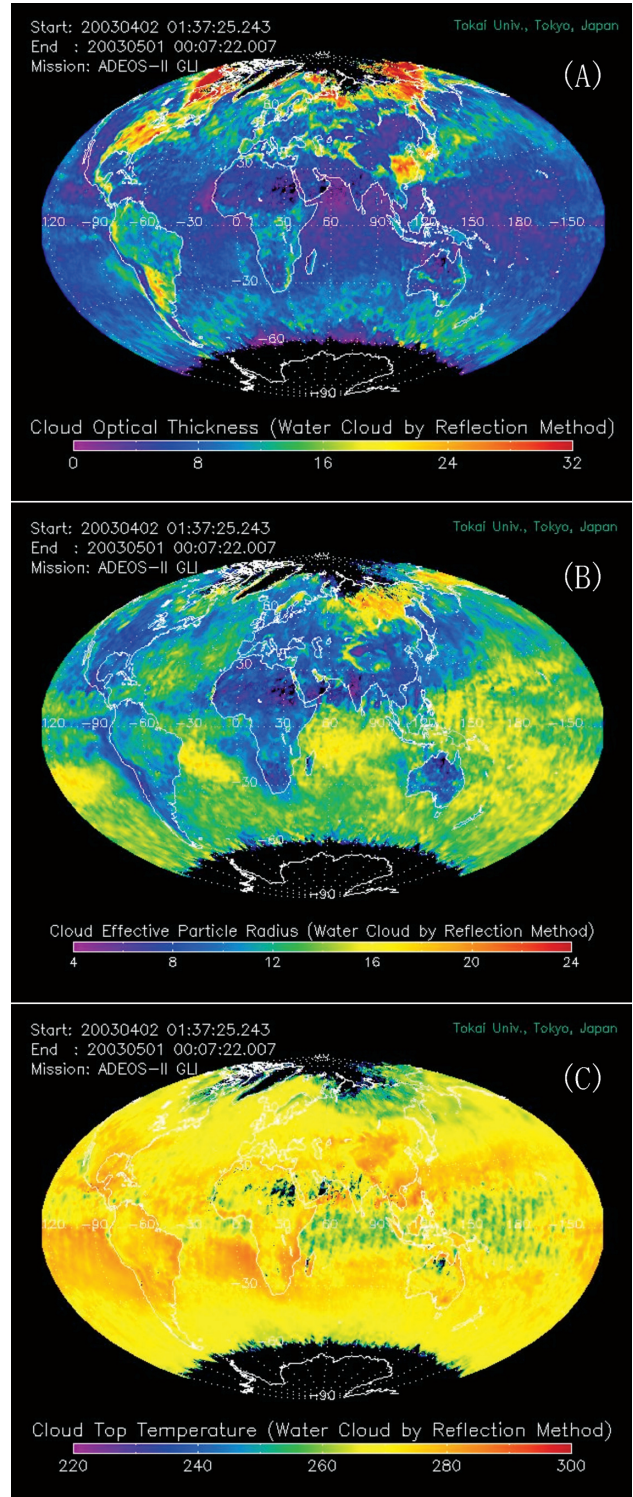

Fig. 3 Cloud parameters averaged over one month, (A) cloud optical thickness, (B) effective particle radius, and (C) cloud top temperature, as obtained from GLI observations in April 2003.

MODIS (~ 6) for land areas, whereas GLI (~ 6) is larger than MODIS (~ 4) for water areas. The shape of the τ_c histogram for water areas indicates that MODIS has more clouds for large τ_c. On the other hand, the r_e histogram is
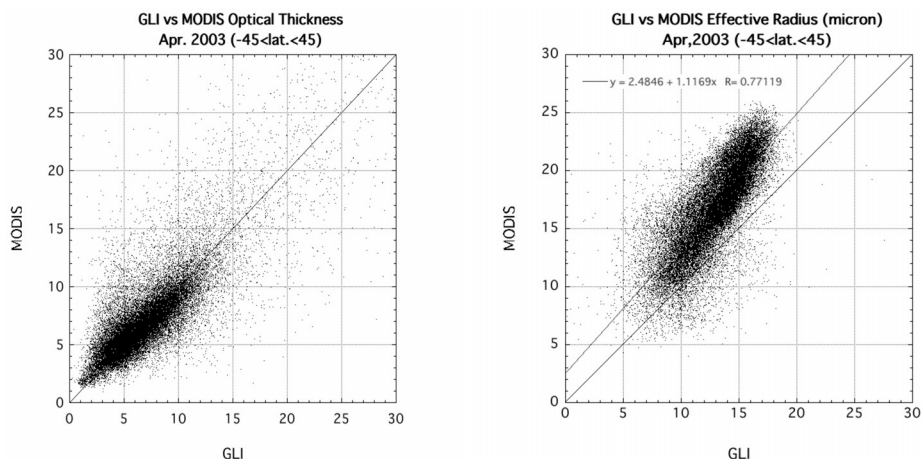
Fig. 4   Correlation between the cloud optical thickness (a) and the effective particle radius (b) as obtained from GLI and MODIS (April 2003) in the latitude domain of 45N to 45S.

quite different, indicating that GLI has a single mode at $12\,\mu$m while MODIS has a bi-modal structure at $10\,\mu$m and $14\,\mu$m as well as that MODIS has an inflection point at $18\,\mu$m (Fig. 5 (b)). Figure 5 (f) shows that this unique structure was intrinsic to water areas. The histogram of r_e from MODIS for water areas shifts to larger regions and is divided into three parts : $5 < r_e < 12\,\mu$m, $12 < r_e < 18\,\mu$m, and $18 < r_e < 25\,\mu$m. This complex structure of the histogram for water areas generated the bi-modal points and the inflection points in the r_e MODIS histogram.

So far, the possible reasons for the differences in the r_e histograms are considered to be (1) poor sensor calibration, especially in the SWIR channels, (2) different SWIR wavelengths used in the measurements, (3) slight differences in the algorithms utilized by GLI and MODIS, such as differences in the treatment of surface reflection, and so on. Among these, (2) is worth inspecting in detail since GLI used a 3.7-μm channel, whereas MODIS used a 2.1-μm channel for the retrieval of r_e. Nakajima et al. (1991)[18], N & N (1995)[7], and Nakajima (2002)[4] suggested that $3.7\,\mu$m and $2.1\,\mu$m wavelengths might retrieve different r_e since the effective depth from the cloud top for $2.1\,\mu$m is deeper than $3.7\,\mu$m due to the different imaginary index of refraction. Thus, the use of two or three channels with the SWIR wavelength retrieves the vertical structure of the particle size in the clouds. For example, if the cloud droplet size in the middle-to-low parts of the cloud layer exhibits larger fluctuations than in the cloud top over the water regions, the MODIS 2.1-μm channel can sense such fluctuations. Thus, it is very important to investigate the retrieved cloud microphysical properties by using active sensors such as radars and/or lidars. All possible reasons mentioned above, including the sensitivity of the wavelength to the effective particle radius, should be examined in detail in future work.

4.3 GLI-AMSR effective particle radius ratio

Figure 6 illustrates the *ERR* as obtained from GLI-AMSR in April 2003. It was found that the covering area of GLI-AMSR is extended to ±60 degrees in latitude. Since the TRMM VIRS-TMI analysis performed by Masunaga et al. (2002b)[13] covers a range of only ±35 degrees, this study presents the first *ERR* results which cover middle-to-high latitude areas. The investigation of clouds over middle-to-high latitudes is important due to the large amount of stratiform clouds forming over these areas[19]. One of the characteristics of this figure is that *ERR* is large over the Middle Pacific Convergence Zone and the South Pacific Convergence Zone (SPCZ), which are known as high precipitation areas. Large *ERR* values indicate that the averaged column effective particle radius is larger than that for the cloud top. This is consistent with the results obtained from the VIRS-TMI analysis performed by Masunaga et al. (2002b)[13]. On the other hand, it is found that the areas of small *ERR* are spread over the North Pacific Ocean, the North Atlantic Ocean, and the Namibian, East Asian, Californian, and Peruvian regions. The effective particle radius of the clouds at the cloud top is comparable to or larger than that at the middle to the bottom layer in these areas. The GLI-AMSR combined analysis is unique since it covers middle-to-high latitude areas, which are not covered by the VIRS-TMI analysis.

5. Discussion and conclusions

The GLI atmospheric science team developed algorithms related to the atmospheric particles and their radiative quantity. Among those algorithms, the ATSK3r algorithm and the GLI-AMSR coupled analysis algorithm, as well as the typical results obtained from these algorithms, were shown in this paper. From the results obtained from ATSK3r, we found
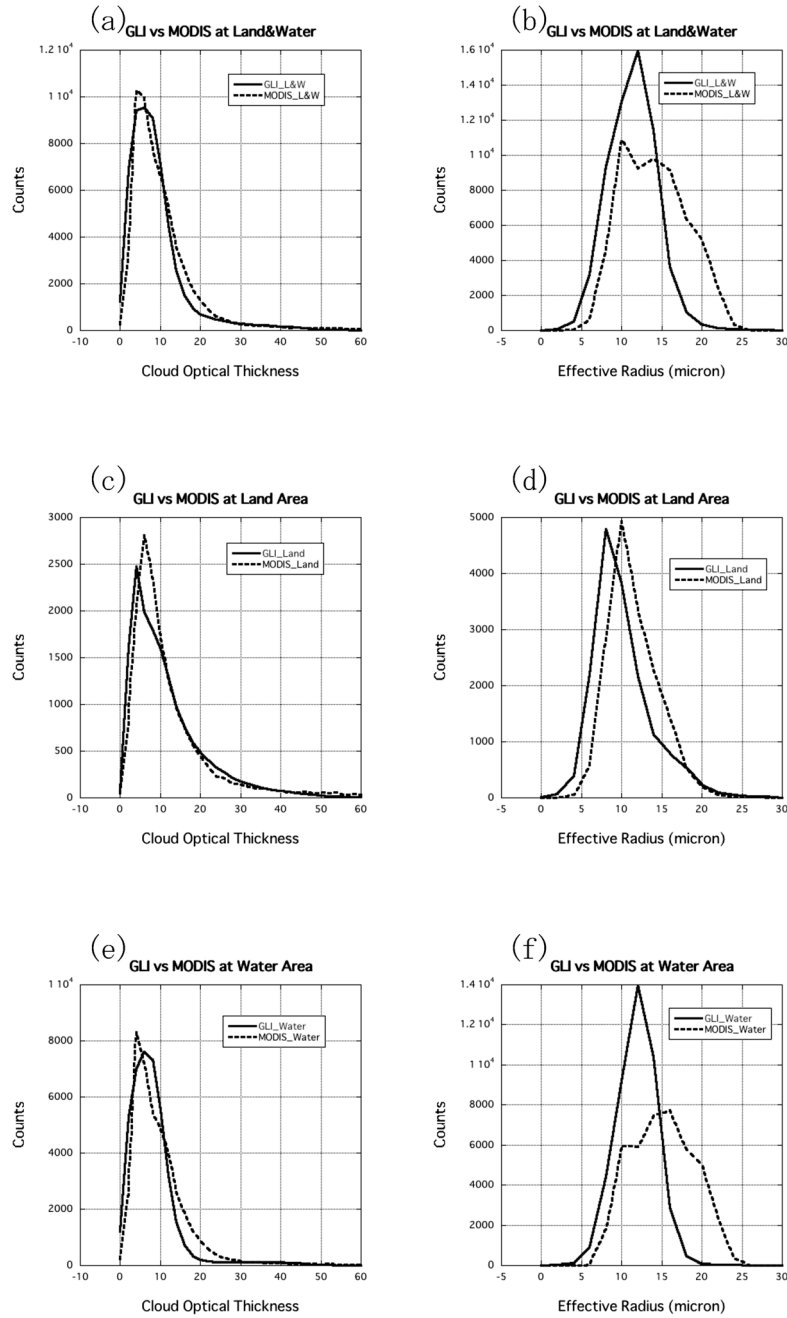
Fig. 5 Histgrams of the cloud optical thickness (left) and the effective particle radius (right) as obtained from GLI and MODIS. (April 2003), for the land and water areas (upper panels), the land areas only (middle), and water areas only (lower).

that the effective particle radius was smaller in continental and coastal ocean areas and larger over open ocean areas. The results are consistent with previous results obtained with other sensors. The results also showed that the areas with small effective particle radius were spread over a wide area of the Middle to North Pacific Ocean. This area corresponds to an area rich in aerosols which come from East Asia, and therefore it is considered that this might be due to indirect effects of environments rich in aerosols.

The effective particle radius as retrieved from MODIS is significantly larger than that from GLI. The comparison of the respective histograms showed that the effective particle radius as derived from GLI had a single mode at $r_e = 12\,\mu$m while that derived from MODIS had a bi-modal structure at $10\,\mu$m and $14\,\mu$m and an inflection point at $18\,\mu$m. This unique shape of the histogram corresponded to measurements over the water area. This finding has created a new opportunity for science activities since the differences in the values of r_e as obtained from GLI and MODIS occurred despite the similar retrieval concepts used in the two sensors. This
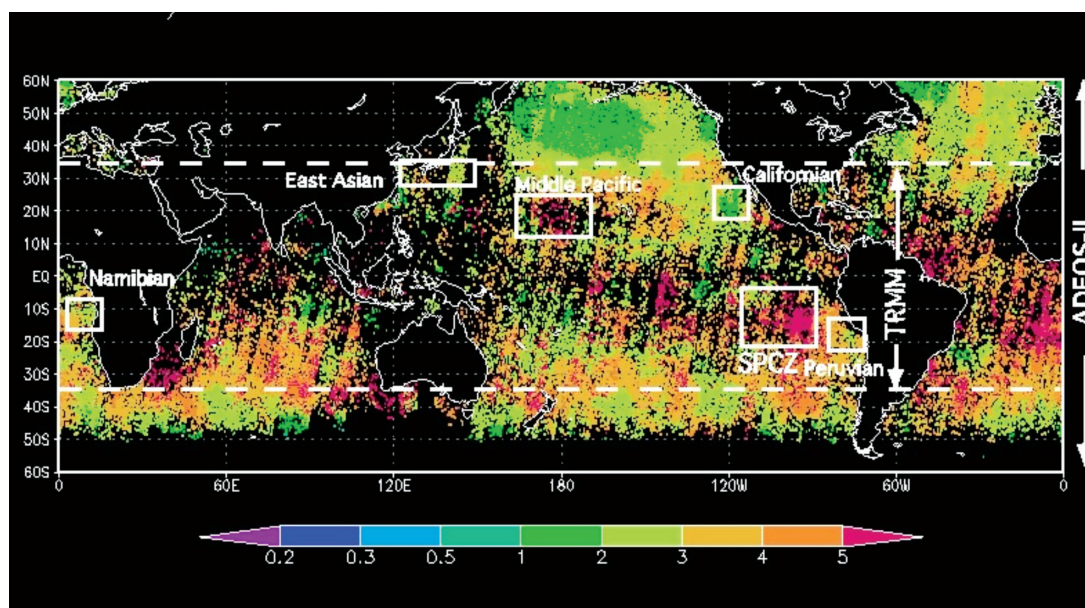
Fig. 6   Effective radius ratio (*ERR*) obtained form the synergistic analysis using GLI and AMSR (April 2003).

implicitly suggests that some unknown factors are still hidden in the radiative transfer or the natural features of the cloud properties. Such exciting research activities are scheduled for future work.

The GLI-AMSR coupled analysis revealed the vertical structure of the cloud effective particle radius over middle-to-high latitude areas for the first time. The results showed that the areas of small effective particle radius ratio are spread over the North Pacific Ocean and the North Atlantic Ocean. This indicates that the effective particle radius near the cloud top is comparable to or larger than that at the middle to bottom layers. Since the obtained results are quite similar at non-precipitation areas, such as the Namibian, East Asian, Californian, and Peruvian regions, where the *ERR* values are relatively small, this constitutes evidence of the suppressed rain formation due to the high concentration of aerosols. In contrast to those non-precipitation areas, the effective particle radius ratio was large over the Middle Pacific and the SPCZ areas, which are known as precipitation areas.

It is noteworthy that there are many extended research efforts regarding cloud observations which contribute to global climate studies. First, the radiation budget can be estimated from the distribution of clouds and the optical properties of aerosols as obtained from GLI[20]. Second, the comparison of the GLI outputs with the model results can be used in assessing the process of cloud droplet growth. For example, Suzuki et al. (2006)[21] developed a non-hydrostatic cloud droplet growth model and simulated the correlation pattern appearing in the NOAA/AVHRR-derived τ_c-r_c scatter plots[7] and showed the typical correlation patterns for pristine and polluted atmospheric environments. Another application

of the cloud observations for model development is the non-hydrostatic cloud resolving model, such as the Non-hydrostatic Icosahedral Atmospheric Model (NICAM) developed by Satoh et al. (2008)[22], who performed global-scale simulations of the cloud distribution with horizontal spatial resolution of 7 km and 3.5 km.

As the model development progresses, more precise surveys of real clouds are needed in order to derive more scientific truths. The datasets of the vertical structure of the effective particle radius which are defined by using, for example, *ERR* and the difference of the effective particle radius obtained through the 3.7- and 2.2-μm channels as mentioned above in this paper might be useful for the further development of these models. Active remote sensing is expected to be another useful technique for investigating the vertical structure of cloud properties. In fact, CloudSat[23] (equipped with a cloud radar) and CALIPSO[24] (equipped with a lidar) as a series of A-Train observations are in operation today, and the launch of the EarthCARE[25] satellite, which is equipped with a cloud radar, a lidar, an imager, and a broadband spectrometer, is planned for 2013. Such active remote sensing systems cover only a very narrow area along their orbit (almost nadir), and therefore the estimation of the cloud properties by using passive imagers is still important for observing the "wide-area" cloud parameters on Earth. Thus, the Global Change Observation Mission (GCOM)-C and GCOM-W, which are equipped with visible-to-infrared imagers and microwave scanners, are planned for launch in the near future. In this regard, this paper suggests innovations with respect to the above points.

References

1) S. Solomon : IPCC (Intergovernmental Panel on Climate Change) (2007), Climate Change 2007 : The Physical Science Basis. Cambridge Univ. Press, Cambridge, UK and New York, USA, 996 pp, 2007.

2) T. Y. Nakajima, T. Nakajima, M. Nakajima, H. Fukushima, M. Kuji, A. Uchiyama, and M. Kishino : Optimization of the Advanced Earth Observing Satellite II Global Imager channels by use of radiative transfer calculations. Applied Optics, 37, 3149–3163, 1998.

3) S. A. Ackerman, S. A., and Richard A. Frey : GLI/MODIS cloud mask results, comparisons, and validation. SPIE, Passive Optical Remote Sensing of the Atmosphere and Clouds IV, Si Chee Tsay, Tatsuya Yokota, Myoung-Hwan Ahn, Editors, December 2004, 17, 2004.

4) T. Y. Nakajima : Development of a comprehensive analysis system for satellite measurement of the cloud microphysical properties, Ph.D. Thesis (University of Tokyo), 131 pp, 2002.

5) M. Kuji, M. and T. Nakajima : Retrieval of cloud geometrical properties using ADEOS-II/GLI data for radiation budget studies. SPIE, Remote Sensing of Clouds and the Atmosphere X, Klaus Schäfer, Adolfo Comerón, James R. Slusser, Richard H. Picard, Michel R. Carleer, Nicolaos Sifakis, Editors , October 2005.

6) Q. Han, W. B. Rossow, and A. A. Lacis : Near-global survey of effective droplet radii in liquid water clouds using ISCCP data. J. Climate, 7, 465–497, 1994.

7) T. Y. Nakajima and T. Nakajima : Wide-area determination of cloud microphysical properties from NOAA AVHRR measurements for FIRE and ASTEX regions. Journal of the Atmospheric Sciences, 52, 4043–4059, 1995.

8) K. Kawamoto, T. Nakajima, and T. Y. Nakajima : A global determination of cloud microphysics with AVHRR remote sensing. Journal of Climate, 14, 2054–2068., 2001.

9) T. Y. Nakajima, A. Uchiyama, T. Takamura, N. Tsujioka, T. Takemura, and T. Nakajima : Comparisons of warm cloud properties obtained from satellite, ground, and aircraft measurements during APEX intensive observation period in 2000 and 2001. Journal of the Meteorological Society of Japan, 83, 1085–1095, 2005.

10) T. Takemura,T. Nozawa, S. Emori, T. Y. Nakajima, and T. Nakajima : Simulation of climate response to aerosol direct and indirect effects with aerosol transport-radiation model. Journal of Geophysical Research-Atmospheres, 110, Doi 10.1029/2004jd005029, 2005.

11) S. Platnick, M. D. King, S. A. Ackerman, W. P. Menzel, B. A. Baum, J. C. Riedi, and R. A. Frey : The MODIS cloud products : Algorithms and examples from Terra. IEEE Transactions on Geoscience and Remote Sensing, 41, 459–473, 2003.

12) H. Masunaga, T. Y. Nakajima, T. Nakajima, M. Kachi, R. Oki, and S. Kuroda : Physical properties of maritime low clouds as retrieved by combined use of Tropical Rainfall Measurement Mission Microwave Imager and Visible/Infrared Scanner : Algorithm. Journal of Geophysical Research-Atmospheres, 107, Doi 10.1029/2001jd000743, 2002a.

13) H. Masunaga, H., T. Y. Nakajima, T. Nakajima, M. Kachi, and K. Suzuki, : Physical properties of maritime low clouds as retrieved by combined use of Tropical Rainfall Measuring Mission (TRMM) Microwave Imager and Visible/Infrared Scanner - 2. Climatology of warm clouds and rain. Journal of Geophysical Research-Atmospheres, 107, Doi 10.1029/2001 jd001269., 2002b.

14) T. Matsui, H. Masunaga, R. A. Pielke, and W. K. Tao : Impact of aerosols and atmospheric thermodynamics on cloud properties within the climate system. Geophysical Research Letters, 31, Doi 10.1029/2003gl019287, 2004.

15) T. Nakajima, and M. Tanaka : Matrix formulation for the transfer of solar radiation in a plane-parallel scattering atmosphere. J. Quant. Spectrosc. Radiat. Transfer, 35, 13–21, 1986.

16) T. Nakajima, and M. Tanaka : Algorithms for radiative intensity calculations in moderately thick atmospheres using a truncation approximation. J. Quant. Spectrosc. Radiat. Transfer, 40, 51–69, 1988.

17) K. Stamnes, S.-C. Tsay, W. Wiscombe, and K. Jayaweera : Numerically stable algorithm for discrete-ordinate-method radiative transfer in multiple scattering and emitting layered media. Appl. Opt., 27, 2502–2509., 1988.

18) T. Nakjaima, M.D. King, J. D. Spinhirne, and L. F. Radke : Determination of the optical thickness and effective radius of clouds from reflected solar radiation measurements. Part II : Marine stratocumulus observations. J. Atmos. Sci., 48, 728–750., 1991.

19) S. A. Klein and D. L. Hartmann : The seasonal cycle of low stratiform clouds, J. Climate, 6, 1587–1606., 1993.

20) T. Takamura, H. Takenaka, Y. Cui, T. Y. Nakajima, A. Higurashi, S. Fukuda, N. Kikuchi, T. Nakajima, I. Sano and R. Pinker : Aerosol and cloud validation system based on SKYNET observations : Estimation of shortwave radiation budget using ADEOS-II/GLI data, J. Remote Sens. Soc. Japan, 29 (1), 40–53, 2009.

21) K. Suzuki, T. Nakajima, T. Y. Nakajima, and A. Khain :

Correlation Pattern between Effective Radius and Optical Thickness of Water Clouds Simulated by a Spectral Bin Microphysics Cloud Model. SOLA, 2, 116–119, 2006.

22）M. Satoh, T. Matsuno, H. Tomita, H. Miura, T. Nasuno and S. Iga : Nonhydrostatic icosahedral atmospheric model (NICAM) for global cloud resolving simulations, J. Comp. Phys., 227, doi : 10.1016/j.jcp.2007.02.006, 2008.

23）G. L. Stephens, D. G. Vane, R. J. Boain, G. G. Mace, K. Sassen, Z. Wang, A. J. Illingworth, E. J. O'Connor, W. B. Rossow, S. L. Durden, S. D. Miller, R. T. Austin, A. Benedetti, C. Mitrescu, and the CloudSat Science Team : The Cloud, Sat mission and the A-TRAIN : A new dimension to space-based observations of clouds and precipitation., Bull. Am. Met. Soc., 83, 1771–1790, 2002.

24）D. Winker, M. Vaughan, and Bill Hunt : The CALIPSO mission and initial results from CALIOP, Proc. SPIE, Vol. 6409, 640902, DOI : 10.1117/12.698003, 2006.

25）H. Kumagai, H. Kuroiwa, S. Kobayashi, and T. Nakajima : Cloud profiling radar for EarthCARE mission, Proc. SPIE, Vol. 4894, 118, DOI : 10.1117/12.469124, 2003.

● **Takashi Y. Nakajima**

Takashi Y. Nakajima received the Doctor of Science degree in "Earth and planetary physics" from Center for Climate System Research (CCSR) of the University of Tokyo in 2002. He came to the Japan Aerospace Exploration Agency (JAXA) in 1994, and moved to Tokai University in 2005. His present researches are remote sensing of clouds and aerosols by using visible and infrared multispectral radiometers, theory of light scattering by non-spherical particles.
E-mail : nkjm@yoyogi.ycc.u-tokai.ac.jp

● **Teruyuki Nakajima**

Teruyuki Nakajima obtained his Dr. of Science degree in geophysics from Tohoku University in 1981. His major research interest is in atmospheric and climate physics. He started his professional career as a teaching assistant, Tohoku University in 1977 ; Assistant professor, Tohoku University, 1981 ; Associate professor at Center for Climate System Research (CCSR), University of Tokyo, 1991 ; now Professor and Director of CCSR. NRC senior visiting associate at NASA/ Goddard Space Flight Center, 1987-1990. President of IAMAS International Radiation Commission, 2004-2008 ; Member of Science Council of Japan. Japan Meteorological Society Award, 1995 and Nissan Science Award, 2000.
E-mail : teruyuki@ccsr.u-tokyo.ac.jp

● **Hirohiko Masunaga**

Hirohiko Masunaga received the Ph.D. degree in astrophysics from the University of Tokyo in 1999. The present affiliation is the Hydropheric Atmospheric Research Center, Nagoya University since 2006. His research interests include cloud and precipitation climatology, tropical climate dynamics, satellite remote sensing, and evaluation of cloud-resolving models.
E-mail : masunaga@hyarc.nagoya-u.ac.jp